EARTH SURFACE PROCESSES AND LANDFORMS
Earth Surf. Process. Landforms **40**, 530–541 (2015)

Published online 11 October 2014 in Wiley Online Library
(wileyonlinelibrary.com) DOI: 10.1002/esp.3652

Field instrumentation for high-resolution parallel monitoring of bedrock erosion and bedload transport

Alexander R. Beer,[1]* Jens M. Turowski,[1,2] Bruno Fritschi[1] and Dirk H. Rieke-Zapp[3]
[1] Swiss Federal Research Institute WSL, Birmensdorf, Switzerland
[2] GFZ German Research Centre for Geosciences, Potsdam, Germany
[3] Institute of Geological Sciences, University of Bern, Bern, Switzerland

Received 20 November 2013; Revised 3 September 2014; Accepted 11 September 2014

*Correspondence to: Alexander R. Beer, Swiss Federal Research Institute WSL, Zürcherstrasse 111, CH-8903 Birmensdorf, Switzerland. E-mail: alexander.beer@wsl.ch

ESPL
Earth Surface Processes and Landforms

ABSTRACT: River incision is fundamental in shaping the Earth's surface. In mountainous regions with steep river beds, fluvial bedrock erosion by bedload transport is an important mechanism forming channels. However, there are only a few complete field datasets that can be used to improve process understanding and evaluate erosion models, especially at the process scale. To provide a simultaneous dataset of hydraulics, bedload transport and bedrock erosion at high temporal and spatial resolution, a new measuring device has been installed in the Erlenbach, a gauged stream in the Swiss Pre-Alps. In this stream, bedload transport rates can be calculated from surveying deposits and from geophone plate sensors and bedload transport samples can be taken directly by an automated moving basket system. To measure bedrock erosion rates simultaneously, two natural stone slabs were mounted flush with the channel bed in a steel frame hosting various measurement devices. Force sensors below the slabs record normal stress and shear stress. At-a-point erosion rates on the slab surfaces are continuously measured at sub-millimetre precision at three locations on each slab. In addition, the slab topography is monitored following erosive flood events. In this article (i) the 'erosion scale' device is described, (ii) data resolution and data quality is assessed by means of tests and event data, and (iii) the first transport event is discussed. The erosion scales are confirmed to provide data at high spatio-temporal resolution for process analysis. The preliminary data show evidence for the tools effect in bedrock erosion. The bedrock slabs can be exchanged to obtain measurements for catchments with different lithologies for comparison. Copyright © 2014 John Wiley & Sons, Ltd.

KEYWORDS: field monitoring; high data resolution; bedload transport; bedrock erosion; tools effect

Introduction

River evolution is a major driver of morphological landscape development. Rivers follow topographic gradients; they adjust and move their bed by removing or depositing material in bedrock and unconsolidated rock channels and export sediment from their catchments. River beds in active orogens are dominated by bedrock channels that are considered key agents in forming mountain geomorphology (Hancock *et al.*, 1998; Whipple *et al.*, 2000; Whipple, 2004; Jansen, 2006). Bedrock channel width, depth and slope, bed roughness, bedrock exposure and sediment size distribution interact under dynamically varying discharge and sediment flux by means of several erosional processes (Wohl, 1998; Johnson and Whipple, 2007; Yanites and Tucker, 2010). Identifying and understanding the rates of the physical processes driving erosion, and how they are affected by material and energy input at highly resolved spatial and temporal scales is fundamental for channel morphodynamics and landscape evolution modelling. In particular, such understanding is essential for transferring these processes to larger spatial scales (e.g. Sklar and Dietrich, 2006).

Erosion of bedrock surfaces can be classified into three main process mechanisms: corrosion (chemical weathering), corrasion (abrasion and plucking/macro-abrasion by impacting sediment particles), and cavitation (implosion damage induced by the collapse of gas bubbles generated by turbulence in the stream) (Hancock *et al.*, 1998; Wohl, 1998; Whipple, 2004; Chatanantavet and Parker, 2009; Whipple *et al.*, 2013). Bedrock morphology is generally linked to these processes: It is thought that plucking is dominant when knickpoints and inner channels are formed, while abrasion is responsible for sculpting the rock and for creating undulations (e.g. Tinkler and Wohl, 1998; Lamb and Fonstad, 2010; Wilson *et al.*, 2013). Except where rocks are relatively soluble, corrosion may be of secondary importance in many bedrock channels (Turowski, 2012). Cavitation is thought to be important only in pothole formation, as it requires high flow velocities that are rare in natural streams (Barnes, 1956; Hancock *et al.*, 1998; Whipple *et al.*, 2000).

Besides climate, channel incision rates are strongly dependent on the lithology of the channel bed and of the transported material (e.g. Whipple *et al.*, 2000; Jansen, 2006; Lamb and Fonstad, 2010). Actual detachment of solid rock, or erosional efficiency, seems to depend on the sediment's tools and cover effects (Gilbert, 1877; Sklar and Dietrich, 1998, 2004; Turowski *et al.*, 2007; Turowski and Rickenmann, 2009). The shielding of bedrock by a sediment layer (the cover effect) limits erosion under high rates of sediment supply (e.g. Turowski *et al.*, 2008; Johnson *et al.*, 2009), whereas the availability of impacting grains

to abrade bedrock (the tools effect; e.g. Foley, 1980) fosters erosion under lower rates of sediment supply (e.g. Finnegan *et al.*, 2007; Cook *et al.*, 2013). Theoretical and laboratory investigations of the process physics have led to the saltation–abrasion model (Sklar and Dietrich, 2004). In this model, erosion rates depend on bed shear stress, on the erodibility of the bedrock (quantified by its tensile strength, its elastic modulus and a dimensionless rock resistance parameter), on the size and impact energy of saltating bedload grains, and on bedload supply relative to transport capacity. Erosion rates thus are explicitly dependent on local sediment transport rates. Peak bedrock erosion rates are thought to occur at moderate bedload supply relative to transport capacity. This is due to the competition of the tools and cover effects (Sklar and Dietrich, 2001; Nelson and Seminara, 2011), and also depends on the maximum saltating grain size (Sklar and Dietrich, 2001, 2004) and on saltation velocity respectively (Chatanantavet *et al.*, 2013), both conditioned by local channel morphology.

Field measurement of bedload transport is a difficult and challenging task due to strong spatial and temporal fluctuations as well as due to the destructive effect of bedload on equipment. Bedload transport rates can be measured with direct methods like hand-held box samplers (e.g. Helley and Smith, 1971), which are mainly used at lower transport rates and deliver data at-a-point in space and time. Temporarily and spatially integrated rates and sediment budgets can be derived from topographic change detection analysis based on repeated surveying (e.g. Lane *et al.*, 1995). In addition, there are surrogate techniques for continuous bedload monitoring that can cover the full range of discharge conditions, but have to be calibrated by direct methods (e.g. Gray *et al.*, 2010; Rickenmann *et al.*, 2014). All available methods have their advantages, disadvantages and restrictions in application and lack of accuracy in space and time, due to extrapolation, interpolation and calibration problems. Geophone-based methods are the most developed surrogate techniques for coarse bedload monitoring (Gray *et al.*, 2010); however, as with all surrogate methods, their field-calibration is challenging.

Similar to bedload transport, fluvial bedrock erosion is difficult to measure, since generally it is a slow process, particularly in resistant substrates (Wohl, 1998). At-a-point, erosion over time has been studied in nature by monitoring (i) borehole depths (Hancock *et al.*, 1998), (ii) heights of erosion pins like nails (Stock *et al.*, 2005) or expansion bolts (Johnson *et al.*, 2010), (iii) by repeated individual point measurements based on fixed benchmarks (Hartshorn *et al.*, 2002; Stephenson, 2013) and (iv) by traditional (Chatanantavet and Parker, 2011) or global positioning system (GPS) survey (Johnson *et al.*, 2009). Field monitoring of whole bedrock surfaces at promising sites have been conducted over several spatial scales using different techniques like aerial photogrammetry and terrestrial laser scanning (TLS; e.g. Cook *et al.*, 2013) for kilometre to centimetre and even to sub-millimetre resolution and accuracy (Rieke-Zapp and Nichols, 2011; Rieke-Zapp *et al.*, 2012; Wilson *et al.*, 2013). However, such measurements have not been paired with bedload transport observations.

Due to the difficulties of obtaining high-quality data, field evaluation of erosion models has so far relied on simplifying assumptions, using long-term erosion rates and sediment yields. In an early paper Foley (1980) inferred the long-term abrasion rate of a glacially diverted stream (Dearborn River, Montana) by dating moraines and estimating corresponding discharge and sediment transport rates by calculations from river geometry and sediment deposits. At the South Fork Eel River, California, basin-averaged paleo-erosion rates were calculated using beryllium-10 (^{10}Be)-concentrations of strath terrace sediments, whose burial age was determined independently by optical-stimulated-luminescence (OSL) dating (Fuller *et al.*, 2009). Strath formation due to extensive sediment cover and lateral erosion could be assigned to elevated sediment supply combined with increasing discharge. Tomkin *et al.* (2003) inferred average erosion rates from strath terrace incision of the Clearwater River, Washington State, assuming long-term steady state conditions and found that none of the six tested erosion models could account for their data. In a comparable attempt using five erosion equations, van der Beek and Bishop (2003) modelled stream evolution from mapped palaeo-channel profiles in the Upper Lachlan catchment, southeast Australia, and concluded that with individual suitable model parameters sets each of the tested models was able to reproduce the current stream profile.

Currently available field data do not allow process and model analysis at high temporal resolution, e.g. on the basis of individual events. In addition, upscaling process-based model formulations to the cross-section, reach or catchment scale is problematic (Turowski and Rickenmann, 2009; Lague, 2010; Turowski, 2012). There is no dataset available of simultaneous measurements of hydraulics, sediment transport, bed forces and bedrock erosion rates for a natural stream (Wohl, 1998) to study their interactions. To fill this gap, we have constructed the 'erosion scales' measuring setup to provide accurate, spatially and temporally high-resolved field data. The aims of this article are (i) to describe the new erosion scale instrumentation, (ii) to evaluate the quality of the data recorded (discharge, bedload transport, erosion), and (iii) to discuss first measurement results and the potential of the equipment for quantitative process studies and evaluation of fluvial bedrock erosion models (cf. Hancock *et al.*, 1998).

The Study Site and its Instrumentation

For more than 30 years the Swiss Federal Institute for Forest, Snow and Landscape Research (WSL) has operated a hydrological field observatory in the Alptal Valley, Canton Schwyz, in the Swiss Pre-Alps (Hegg *et al.*, 2006; Figure 1). There, the Erlenbach stream drains a forested catchment of 0.7 km^2 underlain by Flysch sediments (Winkler *et al.*, 1985; Table I and Figure 2). The transported bedload material is mainly composed of limestone. Stream dynamics and channel morphology of the Erlenbach have been explored in a number of studies (e.g. Schuerch *et al.*, 2006; Turowski *et al.*, 2009; Molnar *et al.*, 2010; Yager *et al.*, 2012; Turowski *et al.*, 2013a).

Previous instrumentation

At the main station, two gauges measure discharge upstream and downstream of a sediment retention basin (Figure 2). Sediment transport observation at the Erlenbach stream date back to 1982, using various methods (Turowski *et al.*, 2009). The entire bedload yield during a specified time interval can be obtained from repeated surveys of the sediment volume in the retention basin (Rickenmann *et al.*, 2012). Bedload transport along the stream channel has been monitored using radio-frequency identification (RFID) tracers (Schneider *et al.*, 2010, 2014). *In situ* bedload samples during a transport event can be taken with a channel-traversing automated bedload sampling system using three 1 m^3 perforated metal baskets operating at a check dam above the retention basin (Rickenmann *et al.*, 2012). Directly upstream of the baskets, passing bedload triggers vibrations on a cross-sectional series of geophone plates (Rickenmann and McArdell, 2007; Turowski *et al.*, 2009; Rickenmann *et al.*, 2012). Plate oscillations induce an electric potential in the attached geophone sensor that is sampled at 10 kHz, but typically summary values (e.g. maximum amplitude) are stored at one minute resolution to reduce data

catchment parameter	Erlenbach stream
contributing area [km^2]	0.7
maximum elevation [m]	1655
minimum elevation [m]	1110
average stream gradient [%]	18
average gradient of the shoot channel [%]	16
gradient of the erosion scales [%]	8
gradient of the geophones [%]	16
stream characterisation	flood-cleaning*
mean annual precipitation [m]	2.30
mean anual temperature [°C]	5
mean annual discharge volume [10^6 m^3]	1.24
mean annual discharge [m^3/s]	0.04
mean annual flood MHQ [m^3/s]	2.00
highest discharge measured [m^3/s]	15‡
mean annual sediment transport [m^3]	480
grain size of 30 weigth per cent d_{30} [m]	0.03
grain size of 50 weigth per cent d_{50} [m]	0.08
grain size of 80 weigth per cent d_{80} [m]	3.00
lithology	flysch
main bedload material	limestone

* Turowski et al., 2013a

‡ 20.06.2007, measurement period 1978-2012, 50year flood

Figure 1. Location of the Erlenbach stream in the Swiss Pre-Alps and its catchment parameters.

volume. The number of signal peaks above a pre-defined threshold, termed impulses, is counted continuously and has been shown to be well correlated with total bedload mass measured with the basket samplers, and with total bedload volumes in the retention basin (Rickenmann *et al.*, 2012, 2014). The signal of the geophones can also be used to calculate the energy transferred to the sensor unit by passing bedload (Turowski *et al.*, 2013b).

The new erosion scales

To further study sediment-flux-driven bedrock erosion during individual discharge events, we developed the 'erosion scales' with the aim of obtaining a coupled dataset of hydraulics, sediment transport and bedrock erosion at high spatio-temporal accuracy. The erosion scale design has partly been adapted from a force plate used for debris flow monitoring at the Illgraben, Canton Valais, Switzerland (McArdell *et al.*, 2007).

The device installed at the Erlenbach hydrological observation site is mounted in a steel frame flush with the streambed of the artificial shoot channel between the upper gauging station and the geophones (Figure 2). It consists of two separate and identical measurement units, i.e. two erosion scales (Figure 3), and is placed 0.3 m upstream and in the streamline of the two central geophone plates. Here the channel gradient flattens gradually to 8% approaching the geophones; the channel mean gradient and the slope of the geophones is 16%, comparable to the natural bed slope of the Erlenbach (Figure 1). Two exchangeable bedrock slabs, each with a width of 0.50 m, a length of 0.36 m in the direction of flow (the same width and length as a geophone plate), and a thickness of 0.06 m are embedded. Each slab is fixed upon four vertical load cells, placed at its four edges, to measure normal forces due to discharge and bedload. Two parallel horizontal force transducers are anchored central below each slab to detect shear forces. It is assumed that passing bedload particles at first hit one of the bedrock slab scales recording normal stress and shear stress, and subsequently stimulate the geophone plate located directly downstream (Figure 3A).

The slabs are exposed to all erosional processes that act upon the streambed. Each slab hosts three integrated upright erosion sensors, adapted from a design of Dubille (2009) (see also Lavé and Dubille, 2011) that detect at-a-point height changes. The sensors consist of thin parallel electrical resistance nets glued into bedrock cylinders of the installed material. Abrasion or plucking on the surface of the slabs and cylinders also cuts inherent wires, resulting in stepwise resistance changes (cf. Berger *et al.*, 2010).

Table I. The dataset obtained from the Erlenbach hydrological observation site, their acquisition frequency, temporal and spatial resolution and estimated accuracy. Further explanations are given in the text

Data source	Data type	Detection method	Detection frequency	Detection resolution	Detection uncertainty[a]
Hydrological observation	Discharge	Control cross-section (upper gauge)	One minute	10^{-3} m^3/s	15%
	(local) Flow velocity	Current meter	Repeated	10^{-1} m/s	5%
	Flow height	Calculation and measurements	Repeated	10^{-2} m	20%
Bedload observation	Accum. bedload volume	TLS basin surveys	Repeated	1 m^3	20% by volume
	Bedload mass samples	Basket samplers	Repeated	2×10^{-1} kg	5% by mass
	Bedload mass transport	Geophone impulses (two central sensors)	One minute[b]	1 kg/one minute[c]	30% by mass
	Bedload volume transport	Geophone impulses (all six sensors)	One minute[b]	1 m^3/event[d]	30% by volume
Erosion observation	Normal stress	Load cells	One minute[b]	6 N/m^2	10%
	Shear stress	Force transducers	One minute[b]	6 N/m^2	10%
	At-a-point surface erosion	Erosion sensors	One minute	10^{-4} m	5%
	Spatial surface erosion	Structured-light 3D surveying	Repeated	10^6 points/m^2	7×10^{-5} m

[a]Rounded up to 5% for uncertainties > 10%; further explanations are given in the text.
[b]Switches to seconds among predefined geophone impulse thresholds.
[c]Above a threshold of 50 impulses and 10 kg bedload transport, respectively.
[d]Above a threshold of 50 000 impulses and 20m3 bedload volume, respectively.

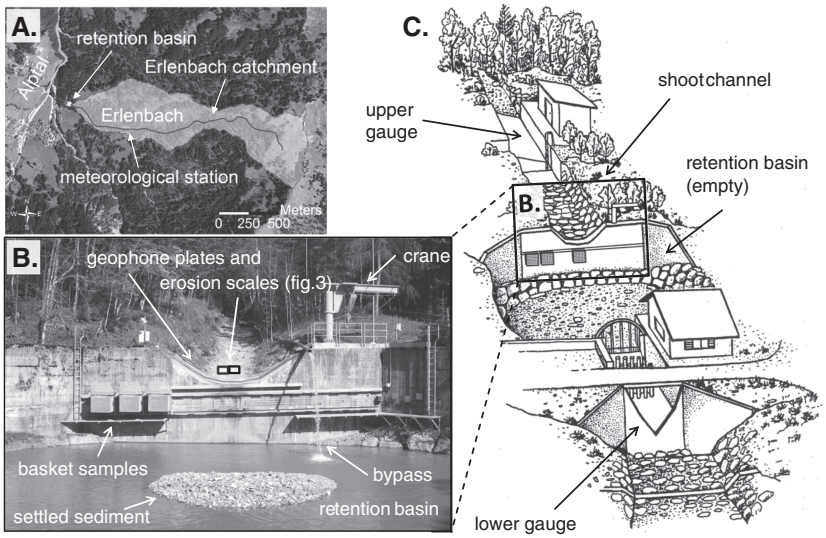

Figure 2. The Erlenbach hydrological observation site: (A) catchment, (B) upstream view of the check dam with the new erosion scales (Figure 3), the geophone plates and the basket samplers in the position ready for sampling. Note the top of the accumulated sediment above the water surface in the retention basin. (C) Sketch of the observatory site showing the full measuring facilities (modified from Baenziger, 1986).

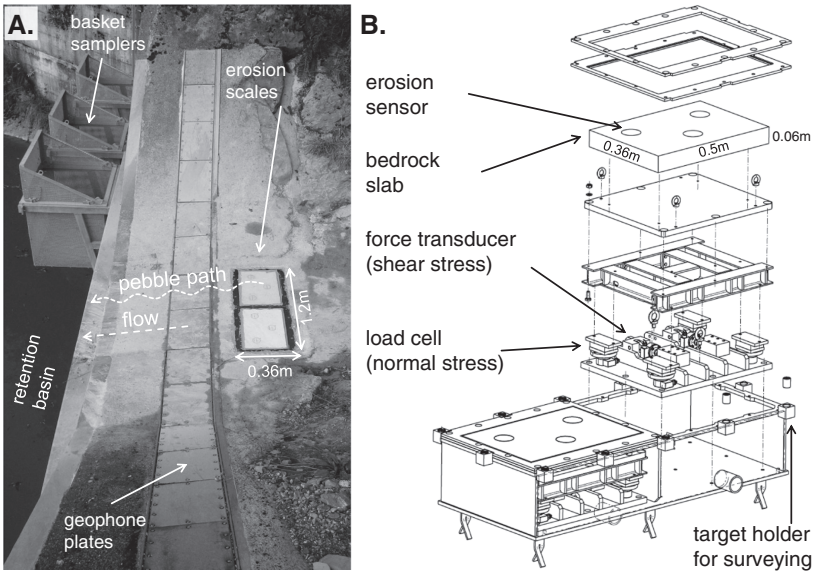

Figure 3. The erosion scales. (A) The steel frame with two stone slabs (marble on the left, concrete on the right in direction of flow) installed flush to the streambed upstream of the geophone plates (see Figure 2B). (B) The sketch of the steel frame showing the structure of the measuring cells for normal and shear stress (technical drawing by H. Herranhof).

In low flow periods (up to the mean annual discharge of 0.04 m^3/s), a mobile bypass structure can be installed to keep the streambed dry (Figure 2B). Hence the whole slab surfaces can be surveyed repeatedly with highly precise and accurate photogrammetry (e.g. Rieke-Zapp and Ebert, 2009; Rieke-Zapp *et al.*, 2012) or structured-light scanning/fringe projection (Akca, 2012; Rieke-Zapp *et al.*, 2012). We briefly describe the experimental protocol later; for more details on both techniques see Luhmann *et al*. (2014). Twelve fixed brass target indicators (FTI; Hubbs, 2014) have been embedded in the steel device (Figure 3B) to host surveying targets for absolute referencing of the resulting digital topography models (DTMs) used for change detection analysis (building DTMs of difference, DoDs). For photogrammetric surveying an Alpa 12 Metric camera was used (Rieke-Zapp *et al.*, 2012), choosing the ground sampling distance to allow for sub-millimetre planimetric spacing of the resulting DTM. A total of around 100 overlapping images were taken in two different configurations. For one-third of the images scale bars and signalized tie points were placed on the surface to create a dense network for camera calibration. By using only a minimum number of these points for automatic orientation and by keeping fixed camera settings, the remaining images were taken with as much of the surface as possible exposed. Combined bundle block adjustment with self-calibration on the job was performed for camera calibration and to establish the exterior orientation of each camera position (cf. Rieke-Zapp *et al.*, 2012). Least squares image matching was then used to automatically generate a dense set of three-dimensional (3D) point measurements on the surface for DTM construction (Gooch *et al.*, 1999). Structured-light scanning surveys with sub-millimetre resolution were conducted using GOM ATOS III or GOM ATOS Compact (GOM, 2014), with some shading of the surface during direct sunlight. In this technique, a projected pattern on the surface is observed by two calibrated cameras and the 3D topography is calculated by triangulation. DTMs and statistics can be built directly in the field using the manufacturer's software.

For first data acquisition and device testing an artificial slab of weak dry-packed concrete (FIXIT 508; Fixit, 2014) was installed together with a Carrara marble slab for potential comparison with erosion rate measurements reported in field and laboratory studies (Sklar and Dietrich, 2001; Hartshorn *et al.*, 2002; Turowski *et al.*, 2008; Sipos *et al.*, 2011; Wilson and Lavé, 2013; Wilson *et al.*, 2013). The concrete slab was replaced in spring 2013 with a serpentinite bedrock slab.

General Data Assessment of the Whole Equipment

In this chapter the technical specifications and estimated detection accuracy of the hydrological, bedload and erosion measurement systems of the Erlenbach site are described (Table I). Uncertainties higher than 10% are quoted in 5% steps. All continuous measurements are monitored with a temporal resolution of one minute. The basket sampler system works above a specific threshold of geophone impulses that can be adjusted for studying different discharge/bedload transport conditions and within a range of discharge defined separately for each basket (Rickenmann *et al.*, 2012). Geophone and stress data are continuously captured with a temporal resolution of one second when a threshold of 20 geophone impulses per second is exceeded.

Discharge

Discharge is measured both at a control cross-section about 35 m upstream of the erosion scales and at a V-notch weir downstream of the retention basin (Figure 2C). The weir was modelled in the laboratory at a scale of 1:6 and its measuring uncertainty was determined to be below 5% up to a discharge of 21 m^3/s (Castellazzi, 1987). The employed rating curve of the upper cross-section was determined with flow velocity data gathered over the course of several decades using dye and salt tracers for discharges up to at least 5 m^3/s. For higher discharges up to 12 m^3/s, the curve was extrapolated from the robust empirical trend and justified by the comparison of the integrated discharge from both gauging stations. However, the details leading to this extrapolation have not been systematically documented and cannot be reconstructed with certainty. Comparison of the integrated discharges from both gauging stations over two years (data resolution of 10 minutes with a maximum discharge of 2 m^3/s) yielded an underestimation of only 2% for the less accurate upper control cross-section; for the event discussed in the present paper it is 1%. Divergences per 10 minutes were below 0.1 m^3/s up to discharges of 1.2 m^3/s. At higher discharges, for which much less data are available, the deviation increased for the upper cross-section and the downstream gauge peaked slightly later. This deviation can be explained by the buffering effect of the retention basin, which damps fast changes in discharge. The damping effect is also visible in the separate gauge level of the basin, indicating comparable peak shifts. Direct comparison (one minute data) of the two discharge measurement series during the event discussed yielded a mean underestimation of 0.5% for the upper control cross-section, with a standard deviation of 5%. Based thereon, the accuracy of the discharge measurements at the upper cross-section, which is subsequently used for analysis, is estimated conservatively at 15%, at least for discharges up to 2 m^3/s. This value results from the rounded up deviation between the upper and the lower gauge plus twice the standard deviation. The estimate accounts for inaccuracies related to water level fluctuations due to turbulence, waves, and bedload transport. At high discharges the rating curve's accuracy may be worse due to fewer available data points and further uncertainties (cf. Domeneghetti *et al.*, 2012).

Flow velocity and flow height

Determination of water flow velocity using dye or salt tracers at the position of the erosion scales is difficult due to a short measuring distance of only 30 m of consistent bed roughness and slope upstream, leading to incomplete mixing. In addition, high flow velocities result in very short transit time of tracer pulses, making precise timing difficult. However, local flow velocity over the erosion scales can be measured using standard current meters with typical accuracies of $< 5\%$ at 0.1 m/s resolution for water depths above 0.05 m (given by manufacturers), if there is no bedload transport. Mean flow velocities can be obtained by integrating measurements at different locations in the flow cross-section. This procedure would introduce additional errors, which are not assessed here. Mean flow height can be calculated based on the cross-sectional geometry from TLS measurements and the width of the actual stream optically extracted from video pictures captured by a camera installed on site. This approach is estimated to have an (conservative) uncertainty of $\pm 20\%$ due to water level fluctuations and its assumed concave cross-sectional surface. Recently a rotating laser distance sensor (SICK TiM551; SICK, 2014) has been installed measuring surface height perpendicular to the stream above the geophones that is able to spatially detect the water surface if turbidity is high enough (above discharges of 0.2 m^3/s). Preliminary analysis promises data quality of flow height and related discharge velocity better than the values given earlier.

Bedload transport

The sediment pile in the retention basin (its top is visible in Figure 2B) is surveyed by TLS with a Leica ScanStation C10 at a mean point resolution of 0.04 m, when the water is drained. On-site scanning precision was determined from a DoD calculated from independent back-to-back scans. The precision is of the order of 1 m^3, which is below 1% by volume uncertainty for typical scan intervals following accumulated sediment delivery above 100 m^3. Converting this to bedload volumes capable of triggering geophone signals, however, is far more uncertain. Some fundamental assumptions need to be made (cf. Rickenmann and McArdell, 2007): (i) a constant proportion of bedload to suspended material over different flood events, (ii) consistent deposition zones in the basin, (iii) sufficiently slow drainage of the retention basin to maintain the sediment pile, and (iv) an even drainage of the sediment pile. Sieve analysis of 17 sediment samples from six individual sampling intervals, taken at different locations of the sediment pile over a period of 30 years give on average 44% by mass of grains larger than 0.02 m in diameter (the standard deviation of this value is 16% by mass), which corresponds to the detection threshold of the geophones (see later). Hence, regarding the TLS precision, accuracy of the bedload grain size threshold from sieve analysis and assuming a constant bulk density, the accumulated sediment volume transported as bedload is given at 20% by volume accuracy. Analysis of a few sediment samples revealed a mean bulk density of 1.75 t/m^3 (Rickenmann and McArdell, 2007; no accuracy available) that can be used for a rough conversion of the volumes to bedload masses.

During sampling the basket samplers are positioned such that they are in line with the two central geophones (Figures 2B and 3A). With a wire mesh spacing of 0.01 m, they can in

theory capture coarse material with 100% efficiency up to a discharge of 6 m^3/s (Rickenmann *et al.*, 2012). However, due to safety and practicability issues they are only used at discharges below 2 m^3/s. Sampling is terminated when a maximal filling of about 200 kg is reached, or after 10 minutes. During approach to and exit from their measuring position, the baskets only partially intercept the stream jet. These periods together do not exceed 10 seconds (Rickenmann *et al.*, 2012), so if a basket stays in the stream jet for 3.5 minutes (the mean of 36 samples), temporal-conditioned uncertainty in full material capture is 3% by mass. This value will increase with decreasing sampling time. The sampled material is sieved using US standard sieves and the size classes are weighed using a crane scale with 0.2 kg accuracy, or a suitable spring balance for small masses. With on average 12 separate weight measurements per basket, error propagation leads to a ceiling uncertainty of 0.7 kg per basket or 1% by mass for sediment diameters > 0.019 m (sieve size). The bedload mass sampling accuracy due to material capture uncertainty and sieving errors is estimated at an upper limit of 5% by mass, since the sieve-dependent grain fraction (0.019 m) is a little lower than the assumed geophone detection threshold of 0.02 m (see later).

The geophone bedload transport monitoring system is an indirect measuring method, the calibration of which strongly depends on sediment shape, motion and on the accuracy of the transported sediment volumes (Turowski and Rickenmann, 2009). The geophone sensors can detect the passage of bedload pebbles with a *b*-axis greater than 0.02–0.04 m (Rickenmann *et al.*, 2012). Sensor output variability decreases with higher transported volumes (e.g. Rickenmann and McArdell, 2007; their data are for the previous sensor generation PBIS [piezoelectric bedload impact sensor], but the process is the same). For further analysis, a bedload detection threshold of 0.02 m is assumed (Rickenmann *et al.*, 2012). We give uncertainties for both mass and volumetric bedload transport rates (Table I), since they originate from different calculations based on the geophone impulses.

Bedload mass transport across the erosion scales can be estimated using the 'basket-regression' of the impulses from the two central geophones (geophones 7 and 8) with trapped bedload from the basket samplers (Rickenmann *et al.*, 2012). A dataset of 34 samples revealed a linear correlation with $R^2 = 0.98$ and a normalized root mean square error (normalized by the standard deviation) NRMSE = 25% by mass for particles > 0.019 m during the short time periods of basket sampling (cf. Rickenmann *et al.*, 2012, equation 1). The estimated accuracy of bedload mass transport is 30% by mass due to the sampling inaccuracy and the deviation between sieved grain fraction diameter (0.019 m) and the assumed 0.02 m geophone detection threshold. The regression holds for data pairs above around 50 impulses or 10 kg respectively, so it can be applied for total bedload masses exceeding this threshold. At the Erlenbach bedload mass transport rates commonly exceed 10 kg/min, and thus bedload transport over the two central geophones can be monitored at minute resolution. Volumetric bedload accumulated over longer periods (whole transport events) can be assessed by an updated version of the 'basin-regression' ($R^2 = 0.99$, NRMSE = 9%; Rickenmann *et al.*, 2012, equation 2) based on the impulses of all six active geophone sensors (sensors 5–10, in the centre of the streambed, Figure 3). This regression holds for more than 50 000 impulses or 20 m^3 and shows a ceiling uncertainty of 30% by volume, considering uncertainties in the detection of bedload volumes from the pile. Thus, long-term volume assessment is possible with this equation, but the data from the retention basin cannot be used for quantitative volumetric transport analysis at minute resolution.

Stresses

Acting forces on top of the erosion scales are assessed by the sum of the output of the corresponding measuring cells, for normal forces HBM C2 – 1000 kg, and for shear forces HBM U2A – 200 kg (HBM, 2014; Figure 3B). Raw data is sampled in parallel with the geophones at 10 kHz and minimum, mean and maximum values are recorded at minute resolution. Normal and shear force measurement accuracy of each slab is better than 1%, using information given by the manufacturer and from laboratory tests with a loading frame prior to field installation. On-site tests of normal stress after slab installation by filling up a water tank confirmed this accuracy for loads up to 2 kN (11 kN/m^2). Field testing shear forces using a spring scale by hand was considerably more difficult and inaccurate, but also resulted in an uncertainty of 1%. However, only a few tests for loads of 0.1 and 0.2 kN were conducted. Both normal and shear forces are recorded at 1 N resolution and are subsequently converted to 6 N/m^2 normal stress and shear stress steps due to the summation of the acting forces over the entire slab surfaces (0.18 m^2 each).

Erosion

The six erosion sensors continuously record at a spatial resolution of 10^{-4} m steps, corresponding to the distance between the wires in the resistance networks. However, an abrasion test with a milling machine on the same electrical measuring setup as used in the field revealed a step resolution of 5×10^{-5} m, which might be due to the structure of the electrical resistance net. The regression function of wire-cut (abrasion) against resistance/voltage change has a R^2 of 0.998 and a NRMSE of 5%.

Both spatial surveying methods, short-range photogrammetry and structured-light scanning, allow for a measurement precision of signalized targets better than 0.05 mm in the configuration used here as specified by the system manufacturers (based on VDI/VDE, 2002). This accuracy was confirmed by the residual error of scan adjustments in a DTM from structured-light scanning. The root mean square error of all point coordinates in the bundle block adjustment of photogrammetry was better than 0.006 mm and residuals in reference points were better than ± 0.01 mm in all dimensions respectively. A DoD of back-to-back measurements of the whole slab surfaces, completely removing and re-assembling the equipment in between, yielded a mean offset of 0.006 mm for both surveying techniques with a standard deviation of ± 0.07 mm.

The First Event

A flood event with a peak discharge of 1.13 m^3/s occurred on 10 October 2011 (Figure 3), shortly after the installation of the erosion scales (3 October 2011). This discharge has a return period of less than one year in the Erlenbach. For the remainder of this paper, we will focus on the stresses and erosion caused by this event on the concrete slab. The purpose of the analysis is both to illustrate the viability of the instrumentation and to present initial observations of the characteristics of acting stresses and erosional signals during a bedload transport event.

The amount of bedload that passed the erosion slabs in two bedload pulses A and B (Figure 4) is estimated at 8.9 t using the basket-regression (or 5.1 m^3 assuming a bulk density of 1.75 t/m^3). TLS of the retention basin was conducted on 22 August 2011 and again on 9 May 2012, giving a total of 21.6 m^3 of sediment (grain diameter > 0.02 m) delivered in this period.

The basin-regression using all geophone impacts for this period yields 22.1 m^3, whereof 19.4 m^3 can be directly assigned to the event of interest here and the remainder to another four smaller discharge events. During the event two basket samplers came into operation. The first sampler entered at 03:05 a.m. and stayed in the stream jet for 591 seconds at a mean discharge of 0.5 m^3/s, while the second entered at 04:59 a.m. and stayed for 124 seconds at a nearly constant discharge of 0.8 m^3/s. They captured 33.8 kg and 111.8 kg of bedload (diameter > 0.019 m), respectively, corresponding to average bedload transport rates of 0.06 kg/s and 0.90 kg/s. During the event, the mean normal stress on the concrete slab increased by 1091 N/m^2 from a minimum of 119 N/m^2 at a discharge of 0.06 m^3/s at midnight to a maximum of 1210 N/m^2 at peak discharge at 09:18 a.m. The mean shear stress record showed only slight activity during most of the event.

However, several simultaneous peaks in both maximal normal stress and minimal shear stress (the maximal amplitudes of the signals downward and downstream) are observable during the second bedload pulse (Figure 5, marked as 'sediment passages?'). Throughout the remainder of the manuscript we will refer to the common occurrence of such peaks as 'peak couples'. The largest peak couple observed in this event (peak steps of 831 N/m^2 and −333 N/m^2) distinctly exceeded the noise of the signals.

Local cumulative abrasion on the concrete slab erosion sensors was 0.15 mm (sensor c1), 0.10 mm (sensor c2) and 0.85 mm (sensor c3) (Figure 4). The accuracy reported here is better than the manufacturer's technical detection resolution (Table I), but is based on the lab-test findings of 0.05 mm resolution (see the section on general data assessment). Abrasion of the sensors mainly occurred during the two bedload pulses (Figure 4), with two consecutive steps of erosion sensor c3 in pulse A and several smaller ones at all three sensors in pulse B (Figure 5). However, these steps did not coincide with peaks of discharge, acting normal stress and shear stress or bedload transport rate. The erosion rate of the whole slab for this event, determined with photogrammetry (Rieke-Zapp *et al*., 2012) was 0.9 mm on average (±0.5 mm) and exceeded 4.6 mm at the upstream edge of the slab (Figure 6). Averaging erosion rates of the slab surfaces around the erosion-sensor point positions c1, c2

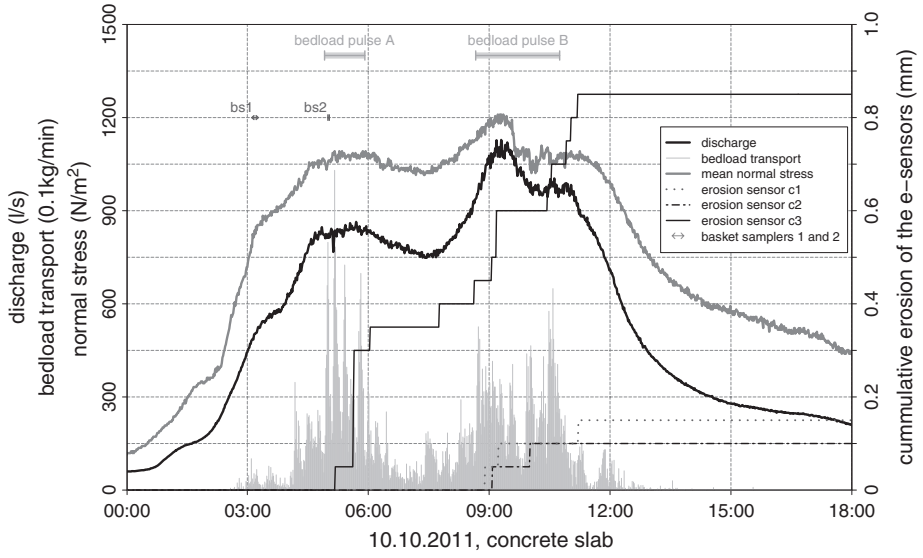

Figure 4. The first erosion event recorded on 10 October 2011. Data is from the concrete erosion slab and geophone 8 located directly downstream. Detail of the indicated sections of bedload pulses A and B in Figure 5, bs1 and bs2 indicate the operation periods of the basket samplers.

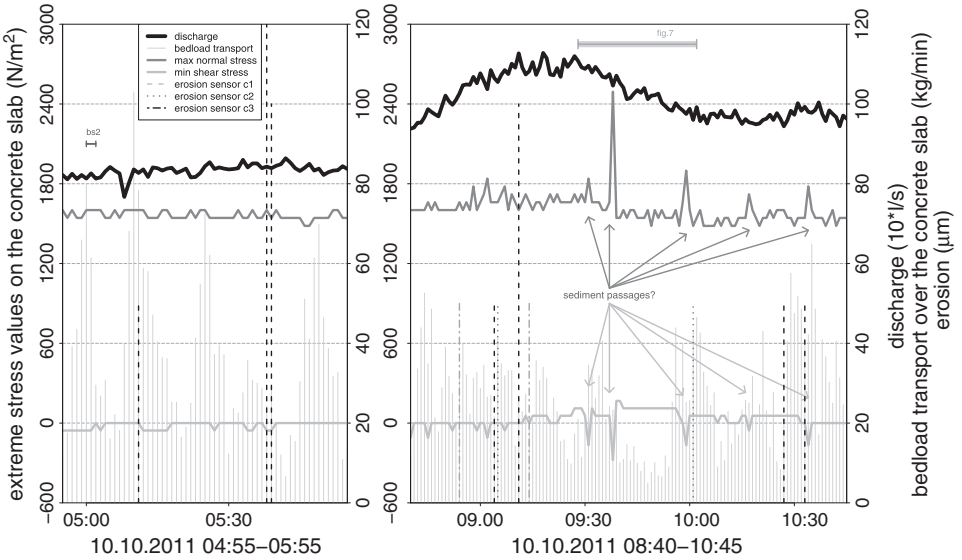

Figure 5. Detail of the bedload pulse sections (A and B) of the 10 October 2011 event (Figure 4) with modified erosion steps on the concrete slab. Minimum shear stress signal is shifted to zero at the time of no discharge ahead of the event for better visibility. Note minimum shear stresses mean highest values in direction of flow. The time segment termed bs2 in (A) is the operation period of bedload basket sampler 2.

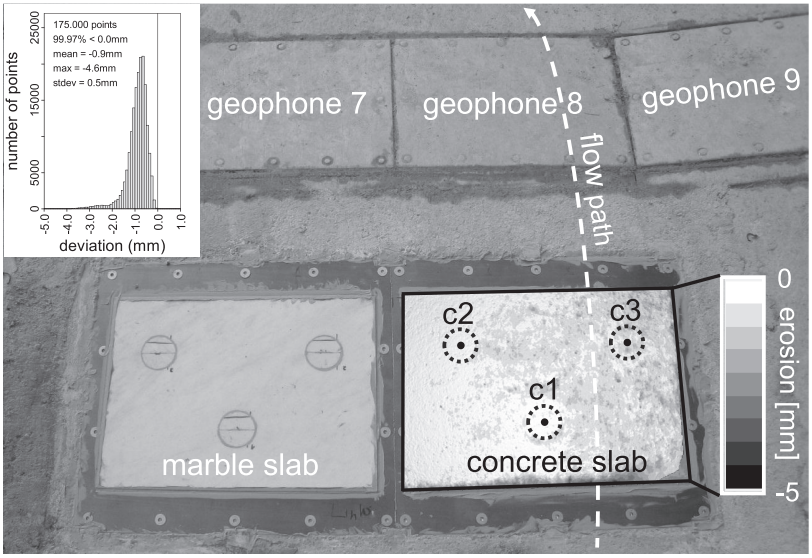

Figure 6. View on the erosion scales in direct of flow. On the left the marble slab with its erosion sensors that were not affected noticeably by the 10 October 2011 flood event. On the right the concrete slab with erosion sensor denotations, their vicinity and a superimposed DoD from photogrammetry showing highest erosion rates at the upstream side (lower part in the picture). A histogram of the spatial deviations from the DoD and related statistics are given in the inset, breaks are in 0.1 mm steps.

and c3 (~20 cm^2 each; indicated by the dashed circles in Figure 6) revealed 0.6 mm (±0.2 mm), 0.4 mm (±0.1 mm) and 1.0 mm (±0.3 mm) of erosion. On the marble slab's erosion sensors no plausible signal was observed.

Discussion

In the following we discuss the actual data quality during the first event, and some specific features and useful insights.

Data quality of the first event

The dataset of the first observed event is assessed following the structure of the general data assessment (Table I) regarding the technical data accuracies mentioned there. This is done to describe the teething troubles of the erosion scale device, and to evaluate and quantitatively confirm its operational functionality.

It can be assumed that the discharge measurement was not disturbed considerably by bedload transport and therefore is reliable. The maximum bedload transport rate was 103 kg/min, or on average 1.7 kg/s at a discharge of 0.8 m^3/s (that is 0.2% by mass of the water flux). The latter corresponds to a water depth of 0.44 m at the gauging level. A single passing spherical grain of 1.7 kg with a density of 2.65 t/m^3 has a diameter smaller than 0.11 m that will not have a strong impact on water stage.

The TLS-derived bedload volume only deviates by 4% by volume from the basin-regression calculation for the longer observation period (22 August 2011 until 9 May 2012) and thus fits well into the regression dataset. The same holds for the bedload mass from basket sampler 1 (bs1 in Figure 4) during the event of interest, which is overestimated by 8% by mass from the basket regression's prediction and for the charge of basket sampler 2 (bs2) with an underestimation of 3% by mass (assuming a constant sediment transport rate over the respective start and end minutes of the baskets runtimes, since the geophone impulses were logged over the whole minutes). The basin-regression overrates the basket-regression volume of the whole event by a factor of 3.8 (19.4 m^3 compared to 5.1 m^3). The divergence between the two regression fits has been discussed by Rickenmann *et al.* (2012), and may be related to the uncertainty in the density of both the transported and deposited bedload, the threshold of detection of the geophone sensors, missed sediment crossing the lateral geophones and the different temporal scales of the measurements.

Due to erroneous data storage, initially only mean normal stress was recorded in 6 N/m^2 steps (Table I). Minimal and maximal steps were logged at 24 N/m^2 and 59 N/m^2 and shear stress was detected at 56 N/m^2, 56 N/m^2 and 556 N/m^2, respectively, for both slabs. The long-term stress signals (especially during low-flow conditions) show a noticeable diurnal course that can be related to discharge, but also to temperature effects on (i) the stone slabs, (ii) the steel frame as well as on (iii) the electronic measuring equipment. However, during the main flood event both slabs were fully covered by turbid water, and water temperature only changed by ± 1 °C, while air temperature rose by 4 °C from midnight to peak discharge (maximum rise of 9 °C, but in the tail of the event; data from NADUF, 2014). Detrending by spectral analysis was not feasible, since discharge and temperature feature the same frequencies. Application of linear regressions damp the daily courses but cause implausible noise in the relation of forces to discharge, potentially due to a (variable) shift between air temperature and stress response. Thus, the raw stress signals were used for analysis here, assuming discharge and bedload transport to be the dominant factors on the signal's performance. The hysteresis in the normal stress signal during the event (Figure 4) might be related to (i) the temperature effects mentioned earlier, (ii) the inaccuracy of the discharge measurements and (iii) possible gauge inertia effective during fast changes of discharge (Figure 4). For compared stress values during times of slow discharge changes, the hysteresis stays within ± 50 N/m^2, corresponding to around 10% accuracy. We used this value as a conservative error estimate for both normal and vertical stress (Table I). A criterion for stress data plausibility is the ratio of shear stress and normal stress that should be close to the slope of the energy line on site or approximately the local bed slope. For the event discussed here this stress ratio is a power function of discharge with an R^2 of 0.98. Above a certain threshold of discharge (around 0.6 m^3/s) with acting stresses exceeding the detection accuracies and resolution steps, the ratio stabilized to lie within a narrow band of 0.06 ± 0.02 m^3/s (with some extreme values enclosing this band by ± 0.05 m^3/s). This is in

good agreement with the inclination of the erosion scales (8%; Table I). Below the threshold the ratio's dependency on discharge is implausible, but can be related to (i) the wider influence of the coarser resolution of the mean shear forces here and (ii) the force-hysteresis, being more distinct below 0.5 m^3/s (Figure 4).

Since storage of the erosion sensor data is on a separate data logger system than discharge, stress and geophone signals, both clocks have to be synchronized regularly. However, this was not implemented until two weeks after the event described here. With a total shift of seven minutes at the moment of synchronization and assuming a constant clock drift, a maximum shift of 2.5 minutes can be attributed to the 10 October 2011 erosion curve and steps (Figures 4, 5 and 7). However, clock drift does not have an influence on the presented analyses.

The erosion sensor data show nearly constant midnight values of the signals before and after the event considered here. Thus, for analysis they were shifted such that a zero value occurs before the flood. The signals feature a diurnal course at a maximum range of 0.15 mm at low flows that may also be due to temperature fluctuations and could be damped only slightly (to maximum 0.1 mm) by regression analysis. Since there are several small scale minute-by-minute fluctuations in the data, plausible erosion steps were determined by smoothing the raw signal to a resolution of 0.05 mm with reference to the milling experiment (Figure 4).

The onset of the erosional signal is delayed from the onset of bedload transport (Figure 4). This could be due to some issues of the sensor construction: (i) the wire patch is pasted on a foil glued into the rock. The topmost wire is aligned flush with the top of the sensor surface by eye and may move during fixing. The wire net is therefore not placed with sub-millimetre accuracy. (ii) As is known from the manufacturer's specifications and laboratory testing, the signal steps from cuts of the uppermost few wires remain below the noise. Thus, the difference between the erosion sensor signals and the surface erosion at the sensor location detected by photogrammetry (Figure 6) is likely due to the initial cut of the top wires, which was not detected by the sensors.

Cumulative surface erosion from slab surveying revealed a plausible and tight normal distribution of local erosion rates (inset in Figure 6) and only a negligible fraction showed positive values of up to 0.6 mm. The latter may be due to surface contamination that is unavoidable during fieldwork even if the slab surface is cleansed repeatedly. The missing bottom right edge of the DoD in Figure 6 is due to missing data.

Some insights from the first event

The bedload flux shows typical strong short-term fluctuations over more than one order of magnitude (Turowski *et al.*, 2009, 2010; Turowski, 2010; Rickenmann *et al.*, 2012; Figure 4). The majority of the bedload mass (79% of the impulses) has been transported across geophone 8 downstream of the concrete slab (Figure 6). Further 19% were recorded on geophone 9 on the right bank. In contrast, geophone 7, downstream of the marble slab, only recorded 0.7% of the entire impulses. This is a common cross-sectional distribution of bedload transport at the Erlenbach stream (Rickenmann and McArdell, 2007) that is due to the flow path across the geophones (sketch of pathway and denotations in Figure 6). However, both geophones 7 and 8 show the same temporal distribution patterns of two bedload pulses accompanied with the two peak stages of the discharge and both recorded some higher bedload transport rates in pulse A (Figures 4 and 5, only for the concrete slab).

In general mean normal stress correlates well with discharge and rose to plausible mean values during the event, independent of the observed hysteresis. However, there is no obvious signal of bedload transport at the rates of discharge and bedload transport considered here (Figure 4). In contrast, the data resolved at second resolution reveal peak couples of the extreme stress values with durations of only one or two seconds distinctly exceeding the hysteresis uncertainty (Figure 5). The first three of these peak couples from maximum normal stress and minimum shear stress occurred at high rates of bedload flux and are most likely due to the passage of individual cobble to boulder sized bedload particles sliding over the slab (Figure 7). This interpretation is supported by the observation that larger pebbles in the Erlenbach are typically angular and elongated.

The cumulative records from the local erosion sensors generally coincide with the courses of discharge and normal stress. In addition, erosion is accelerated during bedload pulses (Figure 4). There is no clear temporal correlation between individual erosion steps and discharge, normal stress or possibly short-time increased sediment transport rates (Figure 5), even if a three minute time-shift of the erosion data is considered. Rather,

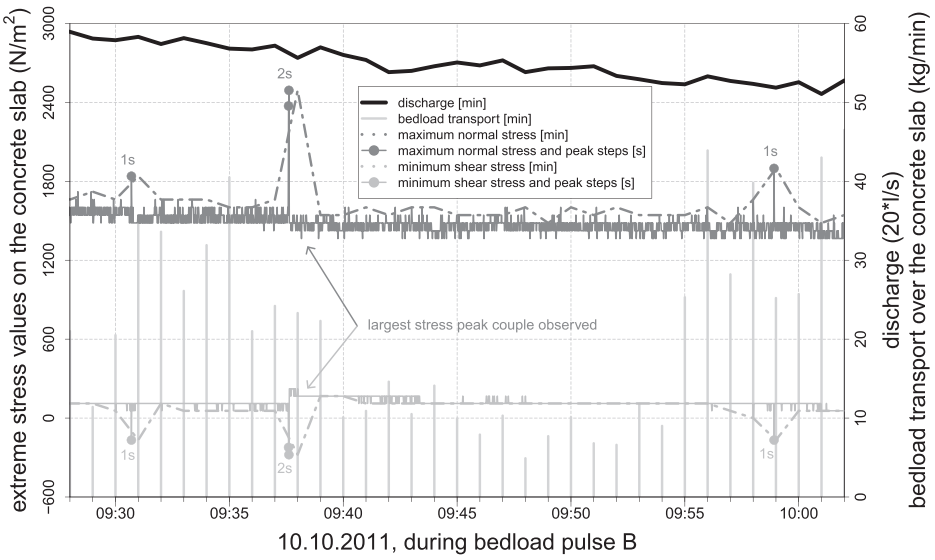

Figure 7. Three stress peak couples (lasting one or two seconds) on the concrete slab during bedload pulse B (see Figures 4 and 5B; shifted force data series like in Figure 5) given in different temporal data resolutions (minutes and seconds). Note minimum shear stresses mean highest values in direction of flow.

these steps can be related to individual local pebble impacts on the exact positions of the erosion sensors acting as erosional tools. Further, the spatial distribution of surface erosion on the concrete slab (Figure 6) shows patterns that are in agreement with this interpretation. From the left to the right side of the slab, seen in direction of flow, there is a strong increase in surface erosion rate magnitude that coincides with the observed flow path of the Erlenbach at this location (Figure 6). Local erosion peaks are due to removal of entire pebbles out of the concrete. Highest spatially distributed erosion rates were detected on the upstream edge of the slab that slightly protrudes out of the steel frame. Here, the initially sharp ridge was rounded and displaced downstream. The ridge exhibits a morphological susceptibility to bedload impacts that exert noticeable normal and shear stresses like the peak couples (Figures 5 and 7). Both types of erosion measurements therefore illustrate the tools effect.

This interpretation is supported by the negligible erosional effect of the small amount of bedload crossing the marble slab. During the event, this slab experienced a mean normal stress span of 433 N/m^2 (40% of the concrete slab's value), but only 83 kg of sediment passed over it, corresponding to 1% of the total mass. The marble data, too, show some stress peak couples and the marble surface had some impact marks. Further, we observed a fine rounding of its protruding upstream right edge similar to that of the concrete slab, vanishing to the left-hand side. However, erosion was detected neither by the marble erosion sensors nor was it visible in the respective DoD. The erodibility of the marble slab is certainly lower than that of the concrete, a fact that is exacerbated by a weak cement layer on top of the concrete slab as a result of suspension settling and water shedding during slab production. Also, the hardness of the Erlenbach's sediment will influence the amplitude of erosion rates on different bedrock materials. Though, despite these factors, the minor erosional rate on the marble slab and its spatial restriction to slab regions with passing bedload provides further evidence for the tools effect in bedrock erosion.

Both erosion measurement techniques applied (erosion sensors and spatial surveying) do not directly allow differentiation between the main erosional processes of abrasion and plucking that may act here. However, the properties of the slab materials (e.g. granularity and brittleness), the cumulative evolution of the erosion sensor signals and the spatial distribution of the slab's surface erosion can be used for interpretation. The discussed event featured a generally continuous evolution of the cumulative concrete erosion sensor records (Figure 4) and total at-a-point erosion is representative for the immediate surroundings of the sensors. Together with the spatially uniform trend to higher erosion values on the concrete slab's right-hand side (Figure 6), this points to abrasion by bedload (and possibly suspended load) as the dominant process. In contrast, the local peak erosion values identified as removal of single grains from the concrete can be classified as plucking.

Conclusions

We have constructed a novel measurement device for collecting a simultaneous dataset of discharge, bedload transport and resulting bedrock erosion in a pre-alpine stream. Both temporal and spatial resolutions of all data types are high and their resolution and accuracy have been assessed by testing and by using real event data. The recorded data are influenced by temperature changes, which currently cannot be corrected for. In future, recording of bedrock slab temperature during transport events might help address this problem. Nevertheless, in general the Erlenbach instrumentation permits quantitative observation of bedload transport, the stress caused by it, energy input to the bed (cf. Turowski *et al.*, 2013b), and associated erosion rates of exchangeable natural bedrock samples. The data for the first event observed provides evidence of the bedload tools effect (after Foley, 1980) on the process scale.

An increased dataset, especially for larger discharge events, will help to improve signal interpretation and correction using filters and spectral analysis. Studies of normal and shear stress measurements as well as associated geophone signals of impacting bedload grains at high temporal resolution could give quantitative insights into the physics of dominant erosion mechanisms (Hancock *et al.*, 1998; Whipple *et al.*, 2000) and allow the calibration of fluvial erosion models used for landscape evolution modelling (Whipple and Tucker, 2002).

Analysis of the Erlenbach's bedload, the installed bedrock slab material and possible replacement with other bedrock could help to upscale and transfer findings to other natural conditions and contribute quantitative datasets to advance the debate of incision model application (e.g. van der Beek and Bishop, 2003; Sklar and Dietrich, 2006). High-resolution measurements of discharge, bedload transport and spatial bedrock erosion allow for testing the hypothesis that sediment transport primarily determines erosion in natural channels through the tools and cover effects (Sklar and Dietrich, 2001; Chatanantavet and Parker, 2008; Cowie *et al.*, 2008), and may illuminate the influence of discharge variability on erosion rates (Turowski, 2012). Additional analysis of the cover effect could be performed, e.g. by artificially covering the erosion slabs and analysing stress data, or by adding known amounts of natural sediment to the stream.

Since the device permits process studies of bedrock erosion it may be further applied to study the relative importance of different erosional processes on overall erosion and their dependencies on bedrock material. Installations of slabs with specific surface topographies could be used for comparison with numerical simulations of acting forces and to monitor roughness evolution (cf. Wilson *et al.*, 2013). Hence, the erosion scales could be a useful tool for quantitative process studies on the importance of bedrock channel formation for mountainous landscape evolution.

Acknowledgements—The authors thank Dieter Rickenmann and Carlos Wyss for fruitful discussions concerning the geophone signals, the Institute of Forensic Medicine, University of Bern for kindly providing their GOM scanner and Lorenzo Campana for field scanning help and advice. The authors are grateful to Jérôme Lavé for support and help with design of the high-resolution erosion sensors adapted from his sensors. The authors further thank Florian Heimann for his comments on an earlier version of the manuscript and Hans Herranhof for the technical implementation of the erosion scales. This study was supported by SNF grant 200021_132163/1.

References

Akca D. 2012. 3D Modeling of Cultural Heritage Objects With A Structured Light System. *Mediterranean Archaeology & Archaeometry* **12**: 139–152.

Baenziger R. 1986. Das Hochwasserereignis vom 25.7.1984 im Erlentobel/Alptal. Interner Bericht G2. *EAFV Wildbach und Hangverbau.*

Barnes HL. 1956. Cavitation as a geological agent. *American Journal of Science* **254**: 493–505.

Berger C, McArdell BW, Fritschi B, Schlunegger F. 2010. A novel method for measuring the timing of bed erosion during debris flows and floods. *Water Resources Research* **46**. DOI: W02502.10.1029/2009WR007993

Castellazzi U. 1987. Hydraulische Modellversuche – Messstation Erlentobel. Eichung des Messuerberfalls der Messstation Erlentobel, Alptal im Modellmassstab 1;6 an der VAW. Interner Bericht V1. *EAFV Wildbach und Hangverbau/Grundlagen.*

Chatanantavet P, Parker G. 2008. Experimental study of bedrock channel alluviation under varied sediment supply and hydraulic conditions. *Water Resources Research* **44**: W12446. DOI: 10.1029/2007WR006581

Chatanantavet P, Parker G. 2009. Physically-based modeling of bedrock incision by abrasion, plucking, and macroabrasion. *Journal of Geophysical Research* **114**: F04018. DOI: 10.1029/2008JF001044

Chatanantavet P, Parker G. 2011. Quantitative testing of model of bedrock channel incision by plucking and macroabrasion. *Journal of Hydraulic Engineering – ASCE* **137**: 1311–1317. DOI: 10.1061/(ASCE)HY.1943-7900.0000421

Chatanantavet P, Whipple KX, Adams MA, Lamb MP. 2013. Experimental study on coarse grain saltation dynamics in bedrock channels. *Journal of Geophysical Research, Earth Surface* **118**: 1–16. DOI: 10.1002/jgrf.20053

Cook KL, Turowski JM, Hovius N. 2013. A demonstration of the importance of bedload transport for fluvial bedrock erosion and knickpoint propagation. *Earth Surface Processes and Landforms* **38**: 683–695. DOI: 10.1002/esp.3313

Cowie PA, Whittaker AC, Attal M, Roberts G, Tucker GE, Ganas A. 2008. New constraints on sediment-flux-dependent river incision: implications for extracting tectonic signals from river profiles. *Geology* **36**: 535–538. DOI: 10.1130/G24681A.1

Domeneghetti A, Castellarin A, Brath A. 2012. Assessing rating-curve uncertainty and its effects on hydraulic model calibration. *Hydrology and Earth System Sciences* **16**: 1191–1202. DOI: 10.5194/hess-16-1191-2012

Dubille M. 2009. Sediment Transport and Abrasion in Bedrock Rivers – From Measurements to Models on an Himalayan Example, PhD Thesis. Joseph Fourier University, Grenoble (in French).

Finnegan NJ, Sklar LS, Fuller TK. 2007. Interplay of sediment supply, river incision, and channel morphology revealed by the transient evolution of an experimental bedrock channel. *Journal of Geophysical Research* **112**: F03S11. DOI: 10.1029/2006JF000569

Fixit. 2014. Trockenbeton 508. http://www.fixit.ch

Foley MG. 1980. Bedrock incision by streams: summary. *Geological Society of America Bulletin, Part II* **91**: 2189–2213. DOI: 10.1130/0016-7606(1980)91577:BIBSS>2.0.CO;2

Fuller TK, Perg LA, Willenbring JK, Lepper K. 2009. Field evidence for climate-driven changes in sediment supply leading to strath terrace formation. *Geology* **37**: 467–470. DOI: 10.1130/G25487A.1

Gilbert GK. 1877. Land sculpture. In *The Geology of the Henry Mountains*. United States Department of the Interior: Washington, DC; chapter V, 99–155.

GOM. 2014. 3D scanner. http://www.gom.com

Gooch MJ, Chandler JH, Stojic M. 1999. Accuracy assessment of digital elevation models generated using the Erdas Imagine OrthoMAX digital photogrammetric system. *The Photogrammetric Record* **16**: 519–531. DOI: 10.1111/0031-868X.00140

Gray JR, Laronne JB, Marr JD. 2010. *Bedload-surrogate Monitoring Technologies*. US Geological Survey: Reston, VA.

Hancock GS, Anderson RS, Whipple KX. 1998. Beyond power: bedrock river incision process and form. In *Rivers over Rock: Fluvial Processes in Bedrock Channels*, Tinkler KJ, Wohl EE (eds). *American Geophysical Union 107*. American Geophysical Union: Washington, DC; 30–60.

Hartshorn K, Hovius N, Dade WB, Slingerland RL. 2002. Climate-driven bedrock incision in an active mountain belt. *Science* **297**: 2036–2038. DOI: 10.1126/science.1075078

HBM. 2014. Load cells. http://www.hbm.com

Hegg C, McArdell BW, Badoux A. 2006. One hundred years of mountain hydrology in Switzerland by the WSL. *Hydrological Processes* **20**: 371–376. DOI: 10.1002/hyp.6055

Helley EJ, Smith W. 1971. *Development and Calibration of a Pressure-difference Bedload Sampler*. US Department of the Interior, Geological Survey, Water Resources Division: Menlo Park, CA.

Hubbs. 2014. FTI targets [online] available at http://www.hubbsmachine.com/, last access: 27 June 2014

Jansen JD. 2006. Flood magnitude-frequency and lithologic control on bedrock river incision in post-orogenic terrain. *Geomorphology* **82**: 39–57. DOI: 10.1016/j.geomorph.2005.08.018

Johnson JPL, Whipple KX. 2007. Feedbacks between erosion and sediment transport in experimental bedrock channels. *Earth Surface Processes and Landforms* **32**: 1048–1062. DOI: 10.1002/esp.1471

Johnson JPL, Whipple KX, Sklar LS, Hanks TC. 2009. Transport slopes, sediment cover, and bedrock channel incision in the Henry Mountains, Utah. *Journal of Geophysical Research* **114**: F02014. DOI: 10.1029/2007JF000862

Johnson JPL, Whipple KX, Sklar LS. 2010. Contrasting bedrock incision rates from snowmelt and flash floods in the Henry Mountains, Utah. *Geological Society of America Bulletin* **122**: 1600–1615. DOI: 10.1130/B30126

Lague D 2010. Reduction of long-term bedrock incision efficiency by short-term alluvial cover intermittency. *Journal of Geophysical Research* **115**: F02011. DOI: 10.1029/2008JF001210

Lamb MP, Fonstad MA. 2010. Rapid formation of a modern bedrock canyon by a single flood event. *Nature Geoscience* **3**: 477–481. DOI: 10.1038/ngeo894

Lane SN, Richards KS, Chandler JH. 1995. Morphological estimation of the time-integrated bed-load transport rate. *Water Resources Research* **31**: 761–772. DOI: 10.1029/94WR01726

Lavé J, Dubille M. 2011. Real-time measurements and modelling of bedrock river erosion along two rivers of the Frontral Himalaya. *Geophysical Research Abstracts* **13**: EGU2011-8108.

Luhmann T, Robson S, Kyle S, Boehm J. 2014. *Close-range Photogrammetry and 3D Imaging*, 2nd edn. Walter de Gruyter: Berlin.

McArdell BW, Bartelt P, Kowalski J. 2007. Field observations of basal forces and fluid pore pressure in a debris flow. *Geophysical Research Letters* **34**: L07406. DOI: 10.1029/2006GL029183

Molnar P, Densmore AL, McArdell BW, Turowski JM, Burlando P. 2010. Analysis of changes in the step-pool morphology and channel profile of a steep mountain stream following a large flood. *Geomorphology* **124**: 85–94. DOI: 10.1016/j.geomorph.2010.08.014

NADUF. 2014. Swiss National River Monitoring and Survey Programme NADUF. http://www.bafu.admin.ch

Nelson PA, Seminara G. 2011. Modeling the evolution of bedrock channel shape with erosion from saltating bed load. *Geophysical Research Letters* **38**: L17406. DOI: 10.1029/2011GL048628

Rickenmann D, McArdell BW. 2007. Continuous measurement of sediment transport in the Erlenbach stream using piezoelectric bedload impact sensors. *Earth Surface Processes and Landforms* **32**: 1362–1378. DOI: 10.1002/esp.1478

Rickenmann D, Turowski JM, Fritschi B, Klaiber A, Ludwig A. 2012. Bedload transport measurements at the Erlenbach stream with geophones and automated basket samplers. *Earth Surface Processes and Landforms* **37**: 1000–1011. DOI: 10.1002/esp.3225

Rickenmann D, Turowski JM, Fritschi B, Wyss C, Laronne JB, Barzilai R, Reid I, Kreisler A, Aigner J, Habersack H. 2014. Bedload transport measurements with impact plate geophones: comparison of sensor calibration at different gravel-bed streams. *Earth Surface Processes and Landforms* **39**: 928–942. DOI: 10.1002/esp.3499

Rieke-Zapp D, Ebert A. 2009. Photogrammetrie mit Shift und Tilt: Nahbereichsanwendungen aus den Geowissenschaften. *Geomatique Suisse* **9**: 452–456.

Rieke-Zapp DH, Nichols MH. 2011. Headcut retreat in a semiarid watershed in the southwestern United States since 1935. *Catena* **87**: 1–10. DOI: 10.1016/j.catena.2011.04.002

Rieke-Zapp DH, Beer AR, Turowski JM, Campana L. 2012. In situ measurement of bedrock erosion. *ISPRS – International Archives of the Photogrammetry, Remote Sensing and Spatial Information Sciences* **XXXIX-B5**: 429–433. DOI: 10.5194/isprsarchives-XXXIX-B5-429-2012

Schneider JM, Hegglin R, Meier S, Turowski JM, Nitsche M, Rickenmann D. 2010. Studying Sediment Transport in Mountain Rivers by Mobile and Stationary RFID Antennas. *5. River Flow 2010*. Bundesanstalt fuer Wasserbau: Karlsruhe; 1723–1730.

Schneider JM, Turowski JM, Rickenmann D, Hegglin R, Arrigo S, Mao L, Kirchner JW. 2014. Scaling relationships between bed load volumes, transport distances, and stream power in steep mountain channels. *Journal of Geophysical Research, Earth Surface* **119**: 533–549. DOI: 10.1002/2013JF002874

Schuerch P, Densmore AL, McArdell BW, Molnar P. 2006. The influence of landsliding on sediment supply and channel change in a steep mountain catchment. *Geomorphology* **78**: 222–235. DOI: 10.1016/j.geomorph.2006.01.025

SICK. 2014. Laserscanner TiM5xx/TiM55x/Outdoor/Short Range. http://www.sick.com

Sipos AA, Domokos G, Wilson A, Hovius N. 2011. A discrete random model describing bedrock profile abrasion. *Mathematical Geosciences* **43**: 583–591. DOI: 10.1007/s11004-011-9343-8

Sklar LS, Dietrich WE. 1998. River longitudinal profiles and bedrock incision models: stream power and the influence of sediment supply. In *Rivers over Rock: Fluvial Processes in Bedrock Channels*, Tinkler KJ, Wohl EE (eds), American Geophysical Union 107. American Geophysical Union: Washington, DC; 237–260.

Sklar LS, Dietrich WE. 2001. Sediment and rock strength controls on river incision into bedrock. *Geology* **29**: 1087–1090. DOI: 10.1130/0091-7613(2001)0291087:SARSCO>2.0.CO;2

Sklar LS, Dietrich WE. 2004. A mechanistic model for river incision into bedrock by saltating bed load. *Water Resources Research* **40**: W06301. DOI: 10.1029/2003WR002496

Sklar LS, Dietrich WE. 2006. The role of sediment in controlling steady-state bedrock channel slope: implications of the saltation–abrasion incision model. *Geomorphology* **82**: 58–83. DOI: 10.1016/j.geomorph.2005.08.019

Stephenson W. 2013. The micro and traversing erosion meter. In *Treatise in Geomorphology: Methods in Geomorphology*, Switzer A, Kennedy DM (eds). Elsevier: Amsterdam; 14.14, 164–169.

Stock JD, Montgomery DR, Collins BD, Dietrich WE, Sklar L. 2005. Field measurements of incision rates following bedrock exposure: implications for process controls on the long profile of valleys cut by rivers and debris flows. *Geological Society of America Bulletin* **117**: 174–194. DOI: 10.1130/B25560.1

Tinkler KJ, Wohl EE. 1998. A primer on bedrock channels. In *Rivers over Rock: Fluvial Processes in Bedrock Channels*, Tinkler KJ, Wohl EE (eds), American Geophysical Union 107. American Geophysical Union American Geophysical Union: Washington, DC; 1–18.

Tomkin JH, Brandon MT, Pazzaglia FJ, Barbour JR, Willett SD. 2003. Quantitative testing of bedrock incision models for the Clearwater River, NW, Washington State. *Journal of Geophysical Research* **108**: 2308. DOI: 10.1029/2001JB000862

Turowski JM. 2010. Probability distributions of bedload transport rates: a new derivation and comparison with field data. *Water Resources Research* **46**: W08501. DOI: 10.1029/2008WR008488

Turowski JM. 2012. Semi-alluvial channels and sediment-flux-driven bedrock erosion. In *Gravel Bed Rivers: Processes, Tools, Environments*, Church M, Biron P, Roy A (eds). John Wiley & Sons: Chichester; 401–416. DOI: 10.1002/9781119952497

Turowski JM, Lague D, Hovius N. 2007. Cover effect in bedrock abrasion: a new derivation and its implication for the modeling of bedrock channel morphology. *Journal of Geophysical Research* **112**: F04006. DOI: 10.1029/2006JF000697

Turowski JM, Hovius N, Hsieh M-L, Lague D, Chen M-C. 2008. Distribution of erosion across bedrock channels. *Earth Surface Processes and Landforms* **33**: 353–363. DOI: 10.1002/esp.1559

Turowski JM, Rickenmann D. 2009. Tools and cover effects in bedload transport observations in the Pitzbach, Austria. *Earth Surface Processes and Landforms* **34**: 26–37. DOI: 10.1002/esp.1686

Turowski JM, Badoux A, Leuzinger J, Hegglin R. 2013a. Large floods, alluvial overprint, and bedrock erosion. *Earth Surface Processes and Landforms* **38**: 947–958. DOI: 10.1002/esp.3341

Turowski JM, Boeckli M, Rickenmann D, Beer AR. 2013b. Field measurements of the energy delivered to the channel bed by moving bedload and links to bedrock erosion. *Journal of Geophysical Reasearch: Earth Surface* **118**: 2438–2450. DOI: 10.1002/2013JF002765

Turowski JM, Yager E, Badoux A, Rickenmann D, Molnar P. 2009. The impact of exceptional events on erosion, bedload transport and channel stability in a step-pool channel. *Earth Surface Processes and Landforms* **34**: 1661–1673. DOI: 10.1002/esp.1855

Turowski JM, Rickenmann D, Dadson SJ. 2010. The partitioning of the total sediment load of a river into suspended load and bedload: a review of empirical data. *Sedimentology* **57**: 1226–1246. DOI: 10.1111/j.1365-3091.2009.01140.x

van der Beek P, Bishop P. 2003. Cenozoic River profile development in the upper Lachlan catchment (SE Australia) as a test of quantitative fluvial incision models. *Journal of Geophysical Research* **108**: 2309. DOI: 10.1029/2002JB002125

VDI/VDE. 2002. *VDI-Richtlinien 2634: Optical 3D measuring systems. Parts 1–3*. Verein Deutscher Ingenieure e.V.: Duesseldorf.

Whipple KX, Hancock GS, Anderson RS. 2000. River incision into bedrock: mechanics and relative efficacy of plucking, abrasion, and cavitation. *Geological Society of America Bulletin* **112**: 490–503. DOI: 10.1130/0016-7606(2000)1120490:RIIBMA>2.3.CO;2

Whipple KX, Tucker GE. 2002. Implications of sediment-flux-dependent river incision models for landscape evolution. *Journal of Geophysical Research* **107**: 2039. DOI: 10.1029/2000JB000044

Whipple KX. 2004. Bedrock rivers and the geomorphology of active orogens. *Annual Review of Earth and Planetary Sciences* **32**: 151–185. DOI: 10.1146/annurev.earth.32.101802.120356

Whipple KX, DiBiase RA, Crosby BT. 2013. Bedrock rivers. In *Treatise in Geomorphology: Methods in Geomorphology*, Switzer A, Kennedy DM (eds). Elsevier: Amsterdam; 550–573.

Wilson A, Lavé J. 2013. The legacy of impact conditions in morphometrics of percussion marks on fluvial bedrock surfaces. *Geomorphology* **186**: 174–180. DOI: 10.1016/j.geomorph.2012.12.033

Wilson A, Hovius N, Turowski JM. 2013. Upstream facing convex surfaces: bedrock bedforms produced by fluvial bedload abrasion. *Geomorphology* **180–181**: 187–204. DOI: 10.1016/j.geomorph.2012.10.010

Winkler W, Wildi W, van Stuijvenberg J, Caron C. 1985. Waegital-Flysch et autres flyschs penniques en Suisse Centrale – Stratigraphie, sedimentologie et comparaisons. *Eclogae Geologicae Helvetiae* **78**: 1–22.

Wohl EE. 1998. Bedrock channel morphology in relation to erosional processes. In *Rivers over Rock: Fluvial Processes in Bedrock Channels*, Tinkler KJ, Wohl EE (eds), American Geophysical Union 107. American Geophysical Union: Washington, DC; 133–151.

Yager EM, Dietrich WE, Kirchner JW, McArdell BW. 2012. Patch dynamics and stability in steep, rough streams. *Journal of Geophysical Research* **117**: F02010. DOI: 10.1029/2011FJ002253

Yanites BJ, Tucker GE. 2010. Controls and limits on bedrock channel geometry. *Journal of Geophysical Research* **115**: F04019. DOI: 10.1029/2009JF001601